Parameter space for a dissipative Fermi–Ulam model

2011 New J. Phys. 13 123012

(http://iopscience.iop.org/1367-2630/13/12/123012)

New Journal of Physics
The open-access journal for physics

Parameter space for a dissipative Fermi–Ulam model

Diego F M Oliveira[1,2] **and Edson D Leonel**[3]

[1] Max-Planck-Institut für Physik komplexer Systeme, Nöthnitzer Strasse 38, D-01187 Dresden, Germany
[2] CAMTP—Center for Applied Mathematics and Theoretical Physics, University of Maribor, Krekova 2, SI-2000 Maribor, Slovenia
[3] Departamento de Estatística, Matemática Aplicada e Computação, Instituto de Geociências e Ciências Exatas, UNESP—Univ Estadual Paulista, Av. 24A, 1515—Bela Vista—CEP: 13506-900, Rio Claro, SP, Brazil
E-mail: diegofregolente@gmail.com and edleonel@rc.unesp.br

New Journal of Physics **13** (2011) 123012 (13pp)
Received 1 August 2011
Published 8 December 2011
Online at http://www.njp.org/
doi:10.1088/1367-2630/13/12/123012

Abstract. The parameter space for a dissipative bouncing ball model under the effect of inelastic collisions is studied. The system is described using a two-dimensional nonlinear area-contracting map. The introduction of dissipation destroys the mixed structure of phase space of the non-dissipative case, leading to the existence of a chaotic attractor and attracting fixed points, which may coexist for certain ranges of control parameters. We have computed the average velocity for the parameter space and made a connection with the parameter space based on the maximum Lyapunov exponent. For both cases, we found an infinite family of self-similar structures of shrimp shape, which correspond to the periodic attractors embedded in a large region that corresponds to the chaotic motion.

Contents

1. Introduction

In an attempt to describe high-energy cosmic rays, Enrico Fermi [1] proposed that a charged particle could be accelerated by interactions with time-dependent magnetic structures. After his pioneering paper of 1949, different versions of the theoretical model were considered, many of which take into account the inclusion of external fields, dissipation, quantum and even relativistic effects [2–8].

One of the most widely studied versions of the problem is the well-known Fermi–Ulam model (FUM). The model is described as being a classical particle confined and bouncing between two rigid walls. One of them is assumed to be fixed and the other moves periodically in time. In the non-dissipative version of the problem, all the collisions with the two walls are assumed to be elastic. The phase space presents a mixed structure in the sense that, depending on the combination of control parameters and initial conditions, invariant spanning curves, chaotic seas and periodic islands are all observed. The presence of the invariant spanning curves limits the unlimited energy gain of the bouncing particle in the chaotic sea; therefore, the phenomenon of Fermi acceleration is not observed. Critical exponents together with a scaling invariance were also characterized in the FUM [8]. A different version of the model in the presence of a gravitational field was proposed by Pustylnikov [9, 10] and it is known as a bouncer [11–13]. It consists of a classical particle bouncing in a vertical moving platform under an external constant gravitational field. Contrary to the FUM, the returning mechanism for a next collision with the moving wall is given only by the gravitational field. Despite their similarities, the bouncer model might show, for specific combinations of both control parameters and initial conditions, the phenomenon of Fermi acceleration, i.e. unlimited energy growth. This surprising result was later discussed and explained by Lichtenberg and Lieberman [14]. Later on, a hybrid version of the FUM and bouncer was proposed [15]. It was shown that properties which are individually characteristic of either the FUM or bouncer models can come together and coexist in the hybrid version of the model.

In this paper, we revisit a dissipative version of the FUM, seeking to understand and describe the parameter space and consequently infinitely many self-similar structures of shrimp shape embedded in the chaotic region. To the best of our knowledge, this is the first time this approach has been applied to such a type of system. The model thus consists of a classical particle confined between two rigid walls. One wall is fixed and the other one moves periodically in time. We assume that the particle experiences inelastic collisions with both walls. We therefore introduce a damping coefficient $\alpha \in [0, 1]$. The limit $\alpha = 1$ recovers all the results for the non-dissipative case. We describe the dynamics of the model via a two-dimensional (2D) nonlinear map with two effective control parameters, namely one dissipation and one perturbation parameter, which also controls the transition from integrability to non-integrability for the conservative case. We show that, once the dissipation is introduced, the mixed structure of the phase space is destroyed and elliptical fixed points turn into sinks and the chaotic sea of the phase space can be replaced by a chaotic attractor [16]. During the investigation, we explore some properties of the parameter space. In particular, we show the existence of self-similar structures called *shrimps*[4].

[4] According to the definition in [17]: 'Shrimps are formed by a regular set of adjacent windows centered around the main pair of intersecting superstable parabolic arcs. A shrimp is a doubly infinite mosaic of stability domains composed by an innermost main domain plus all the adjacent stability domains arising from two period-doubling cascades together with their corresponding domains of chaos. Shrimps should not be confused with their innermost main domain of periodicity.'

Since the pioneering paper of Gallas [18], the parameter space of dissipative models has received special attention and extensive work has been performed considering theoretical models [19–26] (and references therein) and very recently it has also been considered experimentally [27]. A recent result from one of the pioneers of chaos theory, E N Lorenz [28], was also devoted to these intriguing and rich parameter space structures. Here, we have used two approaches to study the parameter space, namely (i) the maximum Lyapunov exponent and (ii) the average velocity over the orbit. The characterization of the Lyapunov exponents has been an important tool used to classify regions in the parameter space as regular (null or negative Lyapunov exponent), or with chaotic behavior (positive Lyapunov exponent), and the behavior of the average velocity has been studied many times to investigate some statistical properties of time-dependent systems [8, 29]. Indeed, in problems where Fermi acceleration is observed, the acceleration is characterized by the growth of the average velocity. Even though the phenomenon of Fermi acceleration is not observed in the FUM because the returning mechanism of the particle for a next collision produces correlation between the collision for high energy and due to the dissipation, a view at the average velocity would be very important and informative as well as complementary to the Lyapunov exponent. In either case, we adopt the following procedure. Starting with a fixed initial condition, for each increment in the parameters we follow the attractor. This means that we use the last value obtained for the dynamical variables before the increment as the new initial condition after the increment. We show that these self-similar structures of shrimp shape are embedded in a region that corresponds to chaotic behavior and they are organized in a particular way.

This paper is organized as follows. In section 2, we provide all the necessary details to obtain the 2D map that describes the dynamics of the system. In section 3, we present and discuss our numerical results. Finally, the conclusions are presented in section 4.

2. The model and the map

In this section, we provide all the necessary details to obtain the map that describes the dynamics of the system. The 1D FUM consists of a classical particle moving between two rigid walls, one of them is assumed to be fixed at $x = l$, while the other one moves periodically in time according to $x_w(t) = \varepsilon \cos(\omega t)$, with velocity $v_w(t) = -\varepsilon\omega \sin(\omega t)$. Here, ε corresponds to the amplitude of oscillation and ω is the frequency of the moving wall. Dissipation can also be introduced by either damping coefficients [16] or in-flight dissipation [29, 30]. However, in this paper we only take into account dissipation due to inelastic collisions. We assume that collisions with both walls are inelastic and the restitution coefficient $\alpha \in [0, 1]$ is introduced when the particle hits the walls. Then there is fractional loss of energy upon collisions. We assume values for α inside the interval (0,1). As is usual in the literature, we describe the dynamics of the system in terms of a 2D map for the variables velocity and time. Thus, after introducing dimensionless variables, the velocity is given by $V_n = v_n/(\omega l)$, the time is measured in terms of the number of oscillations, $\phi_n = \omega t_n$, and $\epsilon = \varepsilon/l$ denotes the dimensionless amplitude of oscillation. Taking into account the above considerations, the 2D map $T(V_n, \phi_n) = (V_{n+1}, \phi_{n+1})$ that describes the dynamics of the system is given by

$$T : \begin{cases} V_{n+1} = V_n^* - (1+\alpha)\epsilon \sin(\phi_{n+1}), \\ \phi_{n+1} = [\phi_n + \Delta T_n] \mod(2\pi), \end{cases} \tag{1}$$

where the corresponding expressions for both V_n^* and ΔT_n depend on what kind of collisions occur, namely: (i) successive collisions and (ii) non-successive collisions. Considering case (i), successive collisions happen after the particle enters the collision zone, $x \in [-\epsilon, \epsilon]$, and experiences a collision with the moving wall; before it leaves the collision zone, the particle experiences a second and successive collisions. Depending on the combination of V_n and ϕ_n, many other successive collisions may happen before the particle leaves the collision zone. In this case, the corresponding expressions for both V_n^* and ΔT_n are given by $V_n^* = -\alpha V_n$ and $\Delta T_n = \phi_c$, where ϕ_c corresponds to the instant of collision and is obtained as the solution of $G(\phi_c) = 0$ with $\phi_c \in (0, 2\pi]$. Here, the function $G(\phi_c)$ is written as

$$G(\phi_c) = \epsilon \cos(\phi_n + \phi_c) - \epsilon \cos(\phi_n) - V_n \phi_c. \tag{2}$$

If the function $G(\phi_c)$ does not have a solution in the interval $\phi_c \in (0, 2\pi]$, it means that the particle left the collision zone and a successive collision is not observed. After some algebra, we show that the determinant of the Jacobian matrix for the case of successive collisions is given by

$$\det(J) = \alpha^2 \left[\frac{V_n + \epsilon \sin(\phi_n)}{V_{n+1} + \epsilon \sin(\phi_{n+1})} \right]. \tag{3}$$

Such a result allows us to conclude that only for the limit case of $\alpha = 1$, the map recovers the property of area preservation for successive collisions. Once the particle has left the collision zone, case (ii) must be taken into consideration. In this case, the corresponding expressions for both V_n^* and ΔT_n used in the map T are $V_n^* = \alpha^2 V_n$ and $\Delta T_n = \phi_r + \phi_l + \phi_c$, where ϕ_r is the time the particle spends traveling to the right-hand side until it hits the fixed wall. After the collision, the particle loses a fraction α of its velocity and is reflected backwards with velocity $-\alpha V_n$. Then, the time the particle spends traveling from the fixed wall until entering the collision zone is ϕ_l. The expressions for both ϕ_r and ϕ_l are written as

$$\phi_r = \frac{1 - \epsilon \cos(\phi_n)}{V_n}, \quad \phi_l = \frac{1 - \epsilon}{\alpha V_n}. \tag{4}$$

Finally, the instant of collision, ϕ_c, is numerically obtained as the solution of $F(\phi_c) = 0$, with $F(\phi_c)$ given by

$$F(\phi_c) = \epsilon \cos(\phi_n + \phi_r + \phi_l + \phi_c) - \epsilon + \alpha V_n \phi_c. \tag{5}$$

In the case of non-successive collision, the determinant of the Jacobian matrix is given by

$$\det(J) = \alpha^4 \left[\frac{V_n + \epsilon \sin(\phi_n)}{V_{n+1} + \epsilon \sin(\phi_{n+1})} \right]. \tag{6}$$

Note that only in the case of $\alpha = 1$ the model is area preserving.

3. Numerical results

In this section, we present and discuss our numerical results for the dissipative FUM. For the conservative case, it is known that the structure of the phase space of the FUM is mixed. However, when dissipation is taken into account, such a structure is changed. Moreover, elliptical fixed points turn into sinks (attracting fixed points). Depending on the range of control parameters, a chaotic sea may be replaced by a chaotic attractor. Figure 1(a) shows a typical

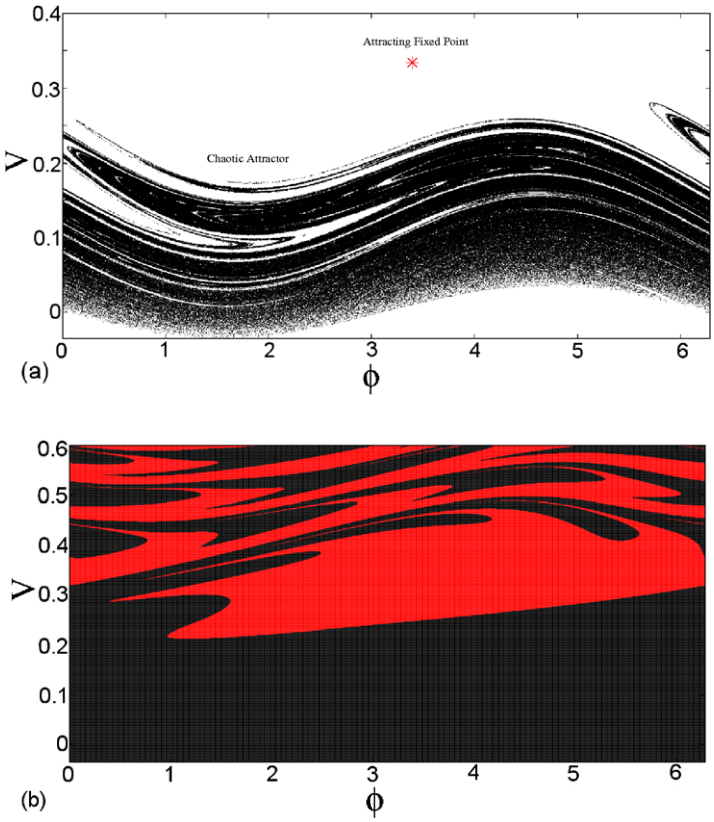

Figure 1. (a) The attracting fixed point for $m = 1$ and a chaotic attractor. (b) Their corresponding basin of attraction. The control parameters used in panels (a) and (b) were $\epsilon = 0.035$ and $\alpha = 0.975$. The region in black corresponds to the basin of attraction of the chaotic attractor, whereas the red region is the basin of attraction for the attracting fixed point.

phase space for the dissipative dynamics of the FUM. We have considered $\alpha = 0.975$ and $\epsilon = 0.035$. For such a combination of control parameters, there are two different attractors: (i) one of them is the attracting fixed point for $m = 1$ and (ii) is a chaotic attractor (see figure 1(a)). The fixed points are obtained from the condition $V_{n+1} = V_n$ and $\phi_{n+1} = \phi_n + 2m\pi$. The solution of these equations gives us that the fixed points are (for further details see [31])

$$V = \left[\frac{1+\alpha}{\alpha^2 - 1}\right] \sin(\phi), \tag{7}$$

$$\phi = \pm \arccos\left[\frac{\epsilon \pm \sqrt{\epsilon^2 + \gamma^2 - 1}}{\epsilon^2 + \gamma^2}\right], \tag{8}$$

where the auxiliary term is defined as

$$\gamma = \frac{2\pi\epsilon\alpha m}{\alpha + 1}\left[\frac{1+\alpha}{\alpha^2 - 1}\right], \tag{9}$$

and $m = 1, 2, 3 \ldots$. One should expect that there must be two different basin boundaries. This is indeed true, as is shown in figure 1(b). The procedure used for obtaining the basin of attraction

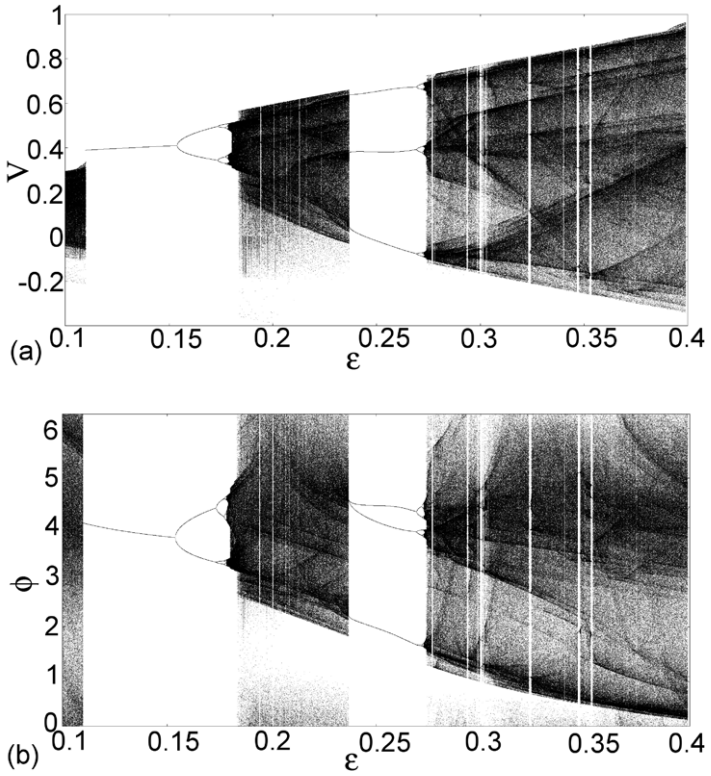

Figure 2. The orbit diagram of (a) V versus ϵ and (b) ϕ versus ϵ for the dissipation parameter $\alpha = 0.77$ and the initial conditions $(\phi_0, V_0) = (3, 10^{-2})$.

for both the chaotic and fixed point attractors consists of iterating a grid of initial conditions in the plane $V \times \phi$ and observing their asymptotic behavior. We have used a range for the initial velocity as $V \in [-\epsilon, 0.6]$ and $\phi \in [0, 2\pi]$. Both the ranges of V and ϕ were divided into 1000 parts each, leading to a total of 10^6 different initial conditions. For such a combination of control parameters, each initial condition was iterated up to 10^5 times. Additionally, we have observed that 65.88% of the initial conditions belongs to the basin of attraction of the chaotic attractor, while the other 34.12% belongs to the basin of attraction of the attracting fixed point. As was reported in [16], increasing the value of the restitution coefficient, which is equivalent to reducing the strength of the dissipation, the chaotic attractor is destroyed, giving place to a chaotic transient. Such an event is called the boundary crisis [32, 33].

To consider the investigation of the parameter space, we vary simultaneously both α and ϵ. However, before doing that, it is interesting to see how the dynamical variables, namely velocity and phase, change as the normalized amplitude of the oscillation of the moving wall ϵ varies for a given dissipation parameter α. Thus, figure 2 shows the behavior of (a) V versus ϵ and (b) ϕ versus ϵ for the dissipation parameter $\alpha = 0.77$ and the initial conditions $(\phi_0, V_0) = (3, 10^{-2})$. As one can see, there are many regions with periodic and chaotic behaviors. The periodic regions evolve into an infinite sequence of bifurcations as ϵ changes. Such a period doubling bifurcation sequence converges geometrically to chaos and Feigenbaum's δ can be obtained [34]. Now, we explore the parameter space by changing both α and ϵ. Here, in order to study the parameter space, we have used two approaches: (i) the maximum Lyapunov exponent and

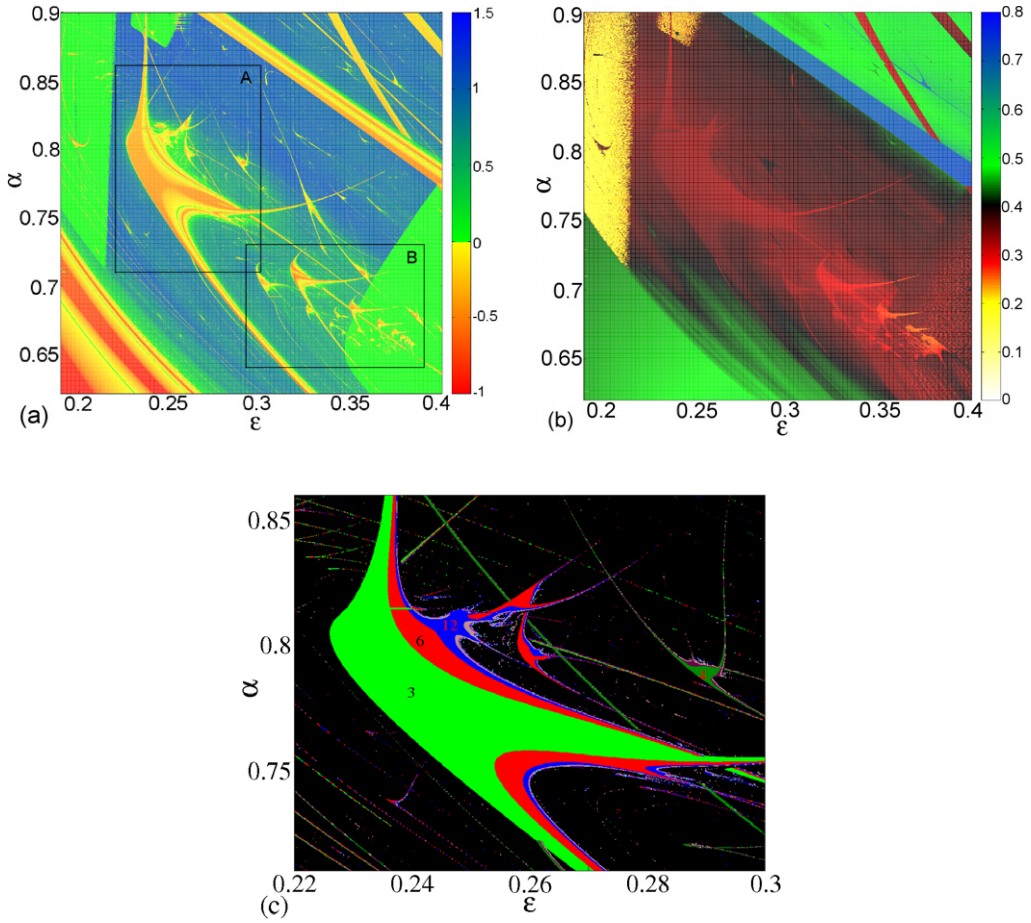

Figure 3. Parameter space for a dissipative FUM for (a) the maximum Lyapunov exponent, where the exponents were coded with a continuous color scale ranging from red-yellow (negative exponents) to green-blue (positive exponents); and (b) the average velocity over the orbit: as one can see, it reproduces qualitatively well the structure shown in (a) for the Lyapunov exponent. (c) Magnification of the main structure in (a); here black indicates chaos (positive Lyapunov exponent) and periodic solutions (negative Lyapunov exponent) are shown in different colors, each indicating a given period: green corresponds to period 3, red to period 6, blue to period 12 and so on.

(ii) the average velocity over the orbit. Considering case (i), we have computed the largest Lyapunov exponent for each combination of (ϵ, α). According to [35], the Lyapunov exponents are defined as

$$\lambda_j = \lim_{n\to\infty} \frac{1}{n} \ln |\Lambda_j|, \quad j = 1, 2, \tag{10}$$

where Λ_j are the eigenvalues of $M = \prod_{i=1}^{n} J_i(\phi_i, V_i)$ and J_i is the Jacobian matrix evaluated along the orbit (ϕ_i, V_i). If at least one of the λ_j is positive, then the system is classified as chaotic. Figure 3 shows the structure of the parameter space for the dissipative FUM. The procedure used to construct the figure was to divide both $\epsilon \in [0.19, 0.4]$ and $\alpha \in [0.62, 0.9]$ into windows of 1000 parts each, leading to a total of 10^6 different initial conditions.

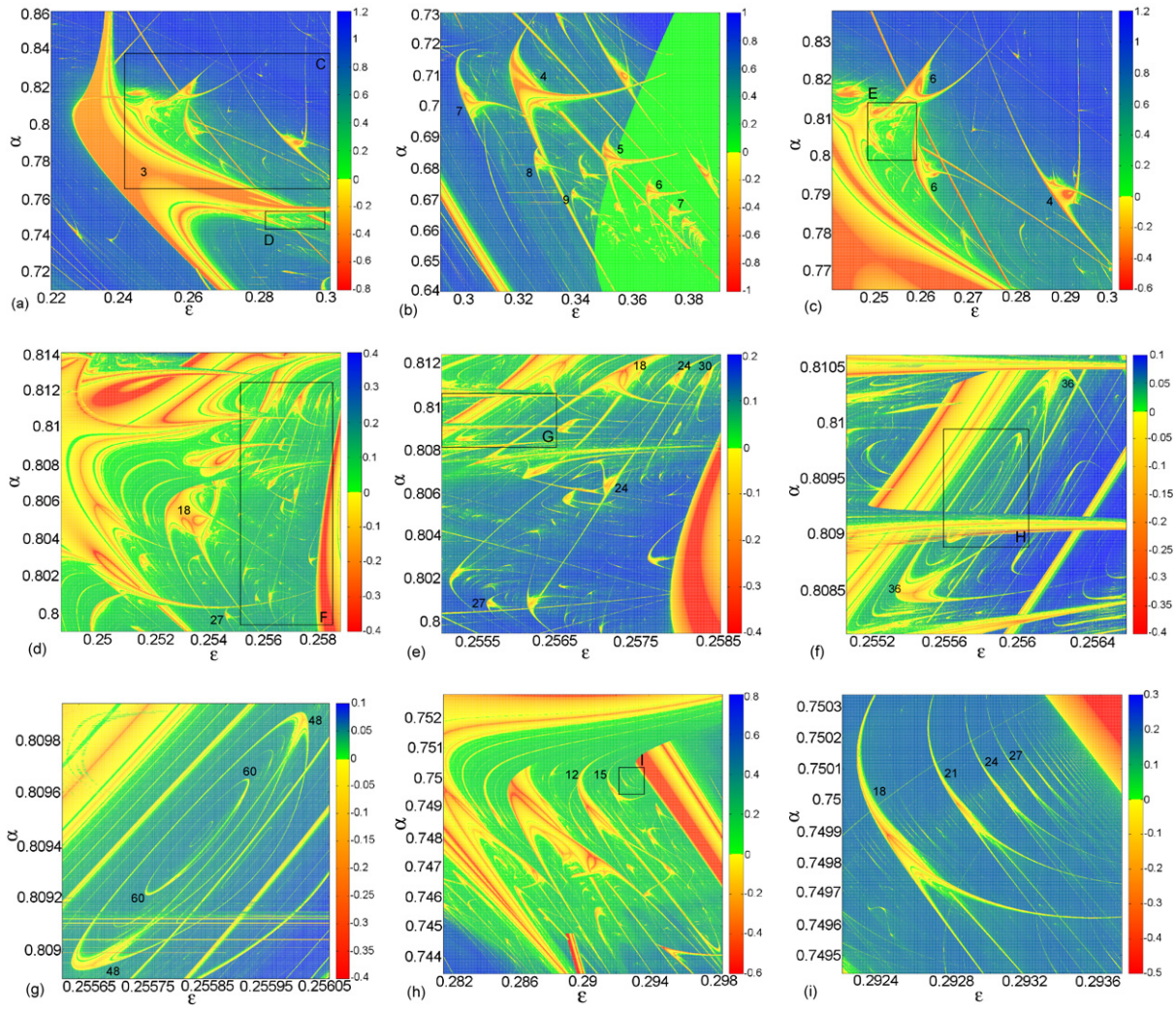

Figure 4. (a, b) Magnification of boxes A and B in figure 3(a); (c) magnification of box C in figure 4(a); (d) the region inside box E; (e) magnification of box F in figure 4(d); (f) magnification of box G in figure 4(e); (g) an enlarged view of box H in figure 4(f); (h) the region inside box D in figure 4(a); and (i) an enlarged view of box I in figure 4(h) where an infinite sequence of shrimps can be observed. The numbering represents the period of the main structure of each shrimp.

Starting with fixed initial condition $(\phi_0, V_0) = (3, 10^{-2})$ (the exception is figure 4(g) where we considered $(\phi_0, V_0) = (6, 10^{-1})$), for each increment in ϵ and α, we follow the attractor. This means that we have used the last pair of values obtained for (ϕ, V) before the increment as the new initial condition after the increment. Such a procedure leads to a loss of information about multiple attractors, since it is possible to attribute only one color to a given combination of control parameters (ϵ, α). In our simulations, we considered a large transient of $n = 10^6$ collisions of the particle with the moving wall and the Lyapunov exponent was computed for the next $n = 10^5$ iterations. The exponents were coded with a continuous color scale ranging from red-yellow (negative exponents) to green-blue (positive exponents), as can be seen in

figures 3(a) and 4. Considering now case (ii), we have studied the parameter space by using the average over the orbit (the ensemble of initial conditions can be used; however, the results are essentially the same), which is

$$\overline{V}(n,\epsilon,\alpha) = \frac{1}{n+1}\sum_{i=0}^{n} V_i. \tag{11}$$

Here, for each combination of (ϵ, α) we have used the same procedure as for the Lyapunov exponent. It is important to emphasize that the unlimited energy growth is not observed in the conservative FUM due to the existence of a set of invariant spanning curves, but even if it was (see an FUM with a random shift in the phase in [36]), the introduction of dissipation is a sufficient condition for suppressing the phenomenon of Fermi acceleration. Therefore, after a transient of $n = 10^7$ we expect a saturation value for the velocity [36] and we compute the average velocity for the next $n = 10^5$ collisions. The result is shown in figure 3(b) and as one can see it reproduces qualitatively well the structure and hence the results for the Lyapunov exponent parameter space (figure 3(a)). It is possible to observe a large shrimp-shaped structure (the same as observed in box A in figure 3(a)) and the sequence of other shrimps observed in box B in figure 3(a). However, it is very hard, even impossible, to distinguish between the chaotic and the regular component, but the parameter space is still extremely rich and exhibits a very intricate structure with many shrimp-shaped domains. Figure 3(c) is a magnification of the main structure in box A in figure 3(a) and colors indicate the period. Each shrimp consists of a main body followed by an infinite sequence of bifurcations following the rule $k \times 2^n$, where k is the period of the main body. In the case of figure 3(c), $k = 3$ and it is shown in green, while red corresponds to period 6, blue denotes period 12 and so on. Chaotic behavior is shown in black.

Figure 4 shows many different regions on the parameter space with magnifications of distinct regions. The color scaling was renormalized from plot to plot. Figure 4(a) shows an enlarged view of the region inside box A in figure 3(a). As has been shown in figure 3(c), there is a main structure of period 3 followed by a sequence of bifurcations. This can also be seen in figure 2 for the same range of ϵ. Figure 4(b) shows a magnification of the region inside box B in figure 3(a), where there are sequences of shrimps (starting with $k = 3$ as shown in figure 4(a) and increasing by a factor of $1:3 \to 4 \to 5 \to 6 \to 7\ldots$) or starting with $k = 7$ and also increasing by a factor of 1 as indicated in figure 4(b). Figure 4(c) is an enlarged view of box C in figure 4(a) where the so-called shrimp twin is observed. It corresponds to two shrimps connected by the leg and it also seems to be connected to half of a third structure. Figure 4(d) is a magnification of box E where very complex and intriguing structures are shown. For example, the structure $k = 18$ shows that several structures coexist as a single body, while there is also the region in box F (shown in figure 4(e)), where a family of shrimps is connected by their 'legs', namely the structures $k = 18$, though it is more clearly evident from looking at the structure $k = 24$ and also $k = 30$. Different from the results presented in [17, 37] for the Rössler oscillator, where the authors observed a family of shrimps connected and spiraling to a center, we observed in figure 4(f) (which corresponds to the region inside box G) two shrimps connected, with $k = 36$, and also many others inside the region of the connected legs, as can be seen in figure 4(g), which is a magnification of box H. Starting from the period of the main structure $k = 36$ it increases by a factor of 12 converging to a center; however, as k increases and the size of the structures decreases, it is no longer possible to differentiate the structures with a shrimp shape from those

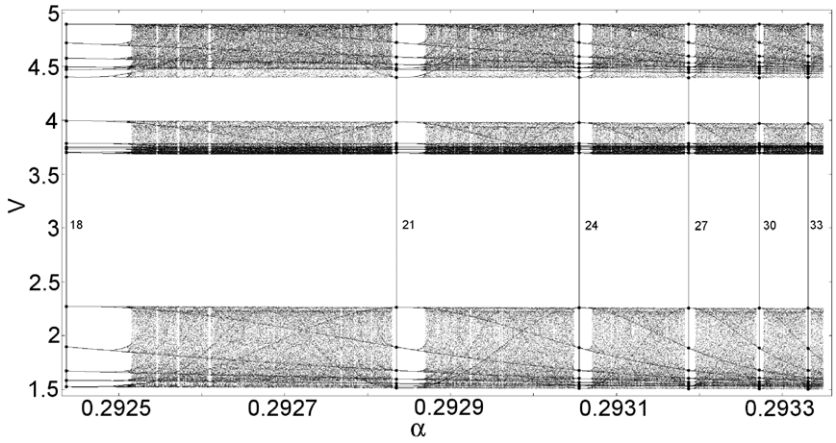

Figure 5. Bifurcation diagram changing simultaneously ϵ and α according to equation (12). Numbers represent the period.

with an elliptical shape. Figure 4(h) corresponds to the region inside box D in figure 4(a), and finally, figure 4(i) corresponds to the region inside box I, where an infinite sequence of shrimps can be observed. Additionally, we observed that they seem to be organized in a very specific direction in the parameter space which can be approximated very well by the equation

$$\alpha = 0.249\,16(7)\epsilon + 0.677\,02(2). \tag{12}$$

Here, 0.000 07 and 0.000 02 correspond to the standard deviation. The procedure we used to obtain equation (12) is to find the region in the middle of each shrimp where the Lyapunov exponent is smaller, for example see the intersection of the four red branches in the structure of $k = 18$ in figure 4(i), and apply a linear fit in the plane (ϵ versus α). Figure 5 shows a bifurcation diagram obtained by changing ϵ and α simultaneously according to equation (12). As one can see, the diagram reflects well the information obtained from figure 4(i) (alternation between chaotic behavior and regular regions) where equation (12) was fitted. The numbers represent the period of the main structure of each shrimp, starting from 18 and increasing by a factor of 3 ($18 \to 21 \to 24 \to 27 \to 30 \to 33 \ldots$). Moreover, a family of infinite shrimps of higher order does exist, as can be seen in figure 4(i) and as confirmed in figure 5.

Let us now discuss more specifically the parameter space constructed for the Lyapunov exponent and for the average velocity. In problems involving Fermi acceleration the natural observable is the average velocity. Although Fermi acceleration is not observed in either the conservative[5] or the dissipative FUM[6], a comparison of the parameter space—where the shrimp-like structures are present—obtained for the Lyapunov exponent and with the average velocity can be used to reinforce the complex organization of the parameter space. Hence the natural observable, which is the average velocity in this case, can be used to observe the shrimp-like formation instead of using the Lyapunov exponent. This is seen better in figure 6, where the plots (a, c) show the corresponding parameter space colored by the Lyapunov exponent value, while plots (b, d) correspond to the same parameter space window but colored by the average velocity

[5] Because of the returning mechanism for a next collision that produces high correlation between the phases at the collisions.

[6] The presence of dissipation leads the phase space to shrink area, therefore creating attractors.

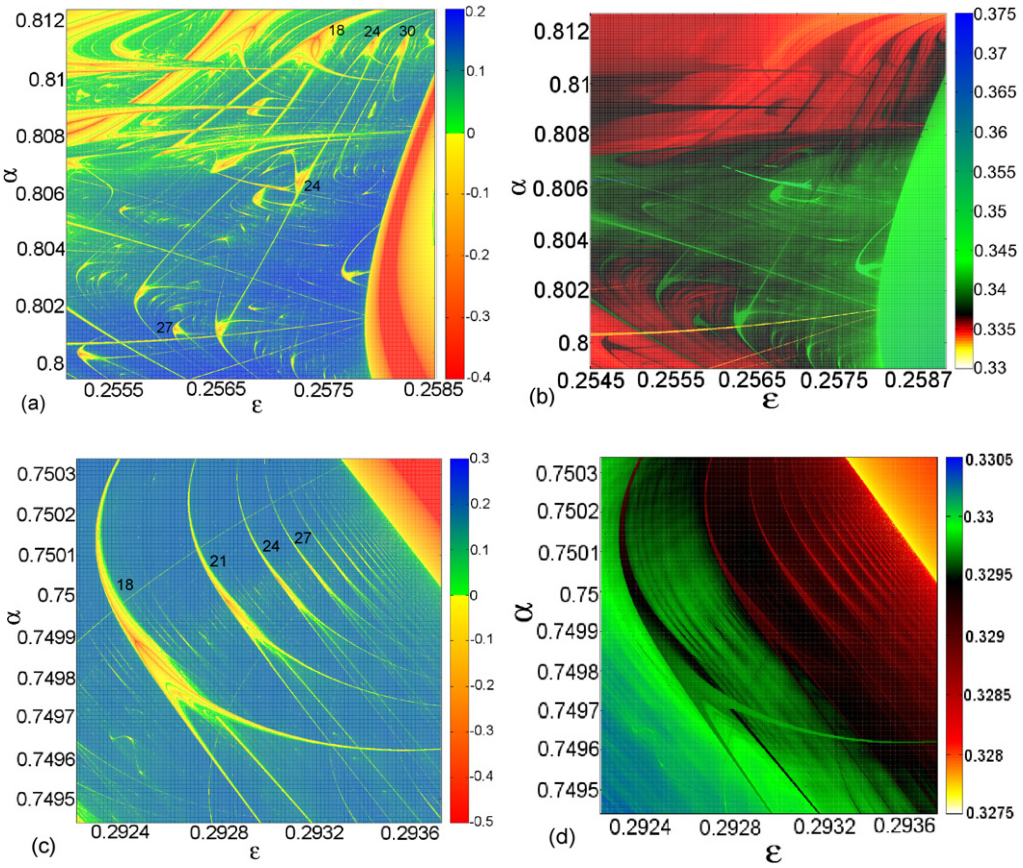

Figure 6. Parameter space for the dissipative FUM where panels (a, c) correspond to the parameter space colored according to the value of the Lyapunov exponent, while panels (b, d) correspond to the same parameter space colored according to the value of the average velocity. The structures observed in both figures for the same range of control parameters are remarkably similar, both qualitatively and quantitatively.

value. The structures observed in both figures for the same ranges are remarkably similar, both qualitatively and quantitatively.

4. Conclusions

In summary, we have studied the Fermi accelerator model considering the introduction of inelastic collisions with both walls. When dissipation is taken into account, the mixed structure of the phase space is changed, the elliptic fixed points are replaced by attracting fixed points and chaotic attractors may appear. We have shown that, by using the maximum Lyapunov exponent and average velocity over the orbit, the parameter space, namely the perturbation parameter ϵ and the dissipation parameter α, presents a very rich structure with an infinite self-similar shrimp shape embedded in a large chaotic region. Our results have shown that they are organized in a particular way in the parameter space and for one specific region, which

can be described according to $\alpha = 0.249\,16(7)\epsilon + 0.677\,02(2)$. The alternation between regular behavior and chaos has been shown in period-adding bifurcation cascades.

Acknowledgments

DFMO gratefully acknowledges financial support from Max-Planck-Institut für Physik Komplexer Systeme and the Slovenian Human Resources Development and Scholarship Fund (Ad futura Foundation). EDL acknowledges financial support from FAPESP, CNPq and FUNDUNESP (Brazilian agencies). The authors also thank Professor J A C Gallas for kindly providing reference [19]. We also thank Eduardo G Altmann for a careful reading of the manuscript. This research was supported by resources supplied by the Center for Scientific Computing (NCC/GridUNESP) of the São Paulo State University (UNESP).

References

[1] Fermi E 1949 *Phys. Rev.* **75** 1169
[2] Lichtenberg A J and Lieberman M A 1992 *Regular and Chaotic Dynamics* (*Applied Mathematical Science* vol 38) (New York: Springer)
[3] Ladeira D G and da Silva J K L 2006 *Phys. Rev.* E **73** 026201
[4] Everson R M 1986 *Physica* D **19** 355
[5] Dembinski S T, Makowski A J and Peplowski P 1993 *Phys. Rev. Lett.* **70** 1093
[6] José J V and Cordery R 1986 *Phys. Rev. Lett.* **56** 290
[7] Leonel E D, da Silva J K L and Kamphorst S O 2004 *Physica* A **331** 435
[8] Leonel E D, McClintock P V E and da Silva J K L 2004 *Phys. Rev. Lett.* **93** 014101
[9] Pustylnikov A D 1983 *Theor. Math. Phys.* **57** 1035
[10] Pustylnikov A D 1995 *Russ. Math. Surv.* **50** 449
[11] Holmes P J 1982 *J. Sound Vib.* **84** 173–89
[12] Everson R M 1986 *Physica* D **19** 355
[13] Leonel E D and Livorati A L P 2008 *Physica* A **387** 1155
[14] Lichtenberg A J, Lieberman M A and Cohen R H 1980 *Physica* D **1** 291
[15] Leonel E D and McClintock P V E 2005 *J. Phys. A: Math. Gen.* **38** 823
[16] Leonel E D and McClintock P V E 2005 *J. Phys. A: Math. Gen.* **38** L425
[17] Vitolo R, Glendinning P and Gallas J A C 2011 *Phys. Rev.* E **84** 016216
[18] Gallas J A C 1983 *Phys. Rev. Lett.* **70** 2714
[19] Gallas J A C 1995 *Appl. Phys.* B **60** S203
[20] Gallas J A C 1994 *Physica* B **202** 196
[21] Hunt B R, Gallas J A C, Grebogi C, Yorke J A and Koçak H 1999 *Physica* D **129** 35
[22] Bonatto C, Garreau J C and Gallas J A C 2005 *Phys. Rev. Lett.* **95** 143905
[23] Bonatto C and Gallas J A C 2008 *Phys. Rev. Lett.* **101** 054101
[24] Albuquerque H A, Rubinger R M and Rech P C 2008 *Phys. Lett.* A **372** 4793
[25] Freire G and Gallas J A C 2010 *Phys. Rev.* E **82** 037202
[26] Celestino A, Manchein C, Albuquerque H A and Beims M W 2011 *Phys. Rev. Lett.* **106** 234101
[27] Stoop R, Benner P and Uwate Y 2010 *Phys. Rev. Lett.* **105** 074102
[28] Lorenz E N 2008 *Physica* D **237** 1689
[29] Oliveira D F M and Robnik M 2011 *Phys. Rev.* E **83** 026202
[30] Leonel E D and McClintock P V E 2006 *Phys. Rev.* E **73** 66223
[31] Leonel E D and Egydio de Carvalho R 2007 *Phys. Lett.* A **364** 475

[32] Grebogi C, Ott C and Yorke J A 1982 *Phys. Rev. Lett.* **48** 1507
[33] Oliveira D F M and Leonel E D 2010 *Phys. Lett.* A **374** 3016
[34] Oliveira D F M and Leonel E D 2008 *Braz. J. Phys.* **38** 62
[35] Eckmann J P and Ruelle D 1985 *Rev. Mod. Phys.* **57** 617
[36] Leonel E D 2007 *J. Phys. A: Math. Gen.* **40** F1077
[37] Barrio R, Blesa F, Serrano S and Shilnikov A 2011 *Phys. Rev.* E **84** 035201